EVIDENCE FOR PROLONGED ACCELERATION BASED ON A DETAILED ANALYSIS OF THE LONG-DURATION SOLAR GAMMA-RAY FLARE OF JUNE 15, 1991

V. V. AKIMOV
Space Research Institute, Moscow 117810, Russia

P. AMBROŽ
Astronomical Institute of the Czech Academy of Sciences, 251 65 Ondřejov Observatory, Czech Republic

A. V. BELOV
IZMIRAN, Troitsk, Moscow Region, 142092, Russia

A. BERLICKI
Astronomical Observatory of Wrocław University, PL 51-622, Wrocław, Poland

I. M. CHERTOK
IZMIRAN, Troitsk, Moscow Region, 142092, Russia

M. KARLICKÝ
Astronomical Institute of the Czech Academy of Sciences, 251 65 Ondřejov Observatory, Czech Republic

V. G. KURT
Institute of Nuclear Physics, Moscow State University, Moscow, 119899, Russia

N. G. LEIKOV
Space Research Institute, Moscow 117810, Russia

YU. E. LITVINENKO
P.K. Shternberg Astronomical Institute, Moscow State University, Moscow, 119899, Russia

A. MAGUN
IAP, University of Bern, CH-3012 Bern, Switzerland

A. MINKO-WASILUK and B. ROMPOLT
Astronomical Observatory of Wrocław University, PL 51-622, Wrocław, Poland

and

B. V. SOMOV
P.K. Shternberg Astronomical Institute, Moscow State University, Moscow, 119899, Russia

(Received 13 January, 1995; in revised form 26 October, 1995)

Abstract. Gamma-ray emission extending to energies greater than 2 GeV and lasting at least for two hours as well as 0.8–8.1 MeV nuclear line emission lasting 40 min were observed with very sensitive telescopes aboard the GAMMA and CGRO satellites for the well-developed post-flare loop formation phase of the 3B/X12 flare on June 15, 1991. We undertook an analysis of optical, radio, cosmic-ray, and other data in order to identify the origin of the energetic particles producing these unusual gamma-ray emissions. The analysis yields evidence that the gamma-rays and other emissions, observed well after the impulsive phase of the flare, appear to be initiated by prolonged nonstationary particle acceleration directly during the late phase of the flare rather than by a long-term trapping of energetic electrons and protons accelerated at the onset of the flare. We argue that such an acceleration, including the acceleration of protons up to GeV energies, can be caused by a prolonged post-eruptive energy release following a coronal mass ejection (CME), when the magnetic field above the active region, strongly disturbed by the CME eruption, relaxes to its initial state through magnetic reconnection in the coronal vertical current sheet.

Solar Physics **166:** 107–134, 1996.

1. Introduction

Observations of the gamma-ray (>200 keV) emission from solar flares is one of the most important tools of the diagnostic of electron and ion acceleration and their interaction with the ambient matter (see Chupp and Walker, 1988; and Ryan and Vestrand, 1994, for a review). The gamma-ray line emission in the 0.2–10 MeV range arises as a result of the ambient matter nuclei excitation by ions with energies of 10–30 MeV nucl^{-1}. The gamma-ray continua are considered either as a result of a high-energy electron bremsstrahlung or as a product of a decay of neutral pions born in interactions of high-energy (>400 MeV) protons with the matter nuclei. The latter process may be recognized by a characteristic shape of the gamma-ray radiation energy spectrum with a broad maximum in the region of 70 MeV.

Due to gamma-ray line observations and their comparison with hard X-ray and microwave bursts, it was discovered that the proton acceleration, at least up to tens of MeV, occurs synchronously with electron acceleration already at the impulsive phase of a flare with a time scale less that 1 s (Forrest and Chupp, 1983). By measurements aboard the SMM and *Hinotori* satellites, the total duration of the gamma-ray line emission did not exceed 20–25 min.

Detection of the continuum gamma-radiation enriched by the neutral pion decay photons was reported for the first time for the June 3, 1982 flare (Forrest *et al.*, 1986). Figure 1 shows that the time profile of the energy release in this flare, as revealed by radio emission at 3 GHz, consists of at least two main components separated by a time interval of about 15 min. The first component (~11:42–11:48 UT) is an impulsive burst with two adjacent peaks and rather sharp decay. There is also the second or delayed component (after ~11:58 UT) with a relatively weak but well visible enhancement. It should be emphasized that for this event the SMM measurements of the gamma-ray continuum with the pion-decay spectrum extending up to 150 MeV (Forrest *et al.*, 1985, 1986) as well as numerous models and simulations (e.g., Ramaty, Murphy, and Dermer, 1987; Kocharov *et al.*, 1988; Gueglenko *et al.*, 1990; Ryan and Lee, 1991; Mandzhavidze and Ramaty, 1992a) belong, in fact, to the two peaks of the impulsive component and its decay phase, but practically do not touch on the delayed component.

The essential progress in the solar flare gamma-ray observations was achieved in 1991, when very sensitive gamma-ray telescopes GAMMA-1 and COMPTEL aboard the GAMMA and CGRO satellites were pointed to the Sun and registered gamma-ray emission in the wide energy range from 0.2 to 2000 MeV. At first, high-energy gamma-ray emission up to several hundred MeV was observed with the GAMMA-1 telescope in the comparatively short-duration flare of March 26, 1991 (Akimov *et al.*, 1991, 1994b). Then, during a period of very high activity associated with AR 6659, a much more powerful and long-lasting flare on June 15, 1991 was observed with the same telescope (Akimov *et al.*, 1991; Leikov *et al.*, 1993). The analysis shows (see below), that this flare had also a two-component time profile of energy release which is very similar to the one of the June 3,

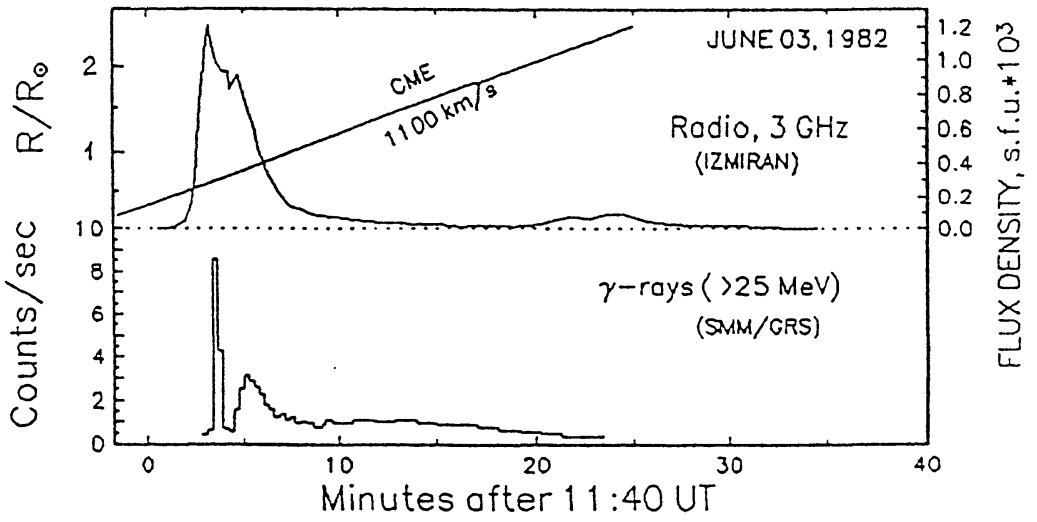

Fig. 1. Microwave and gamma-ray time profiles of the June 3, 1982 flare (Chupp *et al.*, 1985) together with the CME altitude–time trajectory (Sheeley *et al.*, 1985).

1982 flare. However, in this case the gamma-ray continuum, with a clear π°-decay spectrum extending up to unusually high energies of about 2 GeV, was observed just at the time of the delayed microwave component and lasted for more than 2 hours. Moreover, the prolonged gamma-ray line and continuum emission at 1–10 MeV was also registered during ~35 min in the late phase of this flare by the COMPTEL telescope (Ryan *et al.*, 1993). Later, the EGRET team reported even longer (up to 8 hours) high-energy gamma-ray radiation observed during a decay stage of the powerful flare on June 11, 1991 that occurred in the same active region (Kanbach *et al.*, 1993).

A very important and principal question for solar flare physics arises: what is the origin of the energetic particles, in particular, of the GeV protons responsible for such unusual gamma-ray emission well after the impulsive phase? In a number of papers (Mandzhavidze and Ramaty, 1992a, b; Mandzhavidze *et al.*, 1993; Yun-Tung Lau, Northrop, and Finn, 1993) authors, analyzing only the garmma-ray data, showed that the time profiles and the energy spectra of the gamma-ray radiation can be explained in the framework of the same trapping model that has been used successfully for interpretation of the June 3, 1982 flare. In this model, the high-energy ions are accelerated in the short impulsive phase of the flare, subsequently are trapped in coronal magnetic loops, and slowly precipitate into dense matter at the footpoints. On the other hand, the authors did not exclude a model with continuous acceleration and fast precipitation.

A reasonable way to discriminate between the trapping and the continuous acceleration models is to compare the gamma-ray emission with other flare manifestations, in particular to analyze the behavior of particles of different kinds and energies during the late phase of the flare. It is clear, for example, that trapping conditions in coronal magnetic loops and the interaction with plasma turbulence can hardly be the same for such different particles as electrons with energies of

hundreds of keV and several MeV and protons with energies from tens of MeV to several GeV.

The June 15, 1991 flare gives a unique opportunity to compare different data and to identify the origin of the energetic particles responsible for the prolonged high-energy gamma-ray emission well after the impulsive phase. During observations of the gamma-ray emission, radio bursts from millimeter to metric wavelengths were still well-developed and revealed significant variations. The position of the flare on the solar disk (N33 W69) allowed detailed optical observations of the preflare activity, of the two-ribbon flare in Hα and white light as well as the post-flare loop formation. The extremely intense soft X-ray burst of importance X12 was observed although data on hard X-ray emission are not available. Significant flux enhancement of energetic particles in a wide range of energies was registered by the GOES-6, 7 and IMP-8 satellites and by the ground-based neutron monitor network after this flare. In addition, COMPTEL recorded prolonged production of 10–100 MeV neutrons (Debrunner *et al.*, 1993).

The approach outlined above has been applied partly for analysis of the June 15, 1991 flare by Akimov *et al.* (1993, 1994a), as well as by Kocharov *et al.* (1993), although it was restricted mainly to comparison of the gamma-ray and microwave radio data. The preliminary conclusion of these studies was that the model of prolonged particle acceleration is preferable to the model of the long-duration trapping. Akimov *et al.* (1993, 1994a) suggested that the particle acceleration well after the impulsive phase may be related to a long post-eruption energy release after a coronal mass ejection (CME).

In this paper we present more complete and comprehensive analysis of the June 15, 1991 flare by means of comparison of the gamma-ray observations with a whole set of available data indicated above. It should be noted, however, that we do not attempt to consider all interesting features of this unique flare, but will compare only those aspects that may help us answer the main question about the origin of energetic particles producing prolonged gamma-ray emission at the end of the flare.

Similar analysis has been published recently by Kocharov *et al.* (1994).

In Section 2 of our paper we present available experimental data on optical and soft X-ray, radio, gamma-ray and particle observations. In Section 3 we summarize our arguments in favor of the prolonged particle acceleration at the delayed stage of the flare, consider an acceleration mechanism based on the magnetic field restoration after a CME, and show that this mechanism is able to accelerate efficiently protons to tens of GeV energies. At the end, we formulate our conclusions.

2. Observations of the Preflare, Impulsive, and Post-Flare Loop Formation Phases

2.1. Optical and soft X-ray data

The flare of June 15, 1991 was observed in the optical range of the spectrum in mainly the Hα hydrogen line with three solar instruments of the Astronomical Institute of the Wrocław University: the large coronagraph (LC) and solar horizontal telescope (SHT) at Białkow Observatory and the small coronagraph (SC) at Wrocław. A post-flare loop arcade associated with the flare was also observed with a chromospherograph (CH) of the Czech–Croatian Astronomical Observatory at Hvar in the time interval 09:10–15:31 UT. The X-ray emission in two channels (0.5–3.6 Å and 1–8 Å) was obtained from GOES-7 data.

2.1.1. *Preflare Phase*

The onset of the flare was preceded by a huge flaring arch or a huge surge of Rompolt's Class B (Rompolt, 1982; Rompolt and Švestka, 1994). The ejection of material in this arch occurred in the active region NOAA 6659 (AR) that on June 15 was located very close to the west limb. The material was injected into the leg of a huge magnetic arch anchored in the northern part of the AR at around 07:24 UT. A later phase of material propagation along the flaring arch is shown in Figure 2(a). The event ended when the material, after reaching the top part of the arch, flowed completely down along both its arms at around 08:05 UT, very close to the time of start of the large 3B/X12 flare. The arch as seen by the LC consisted of a number of twisted fine filaments (cf., Figure 2(b)). The height of the top part of the flaring arch was 75 000 km above the photosphere (above the AR, assuming that the plain of the arch was perpendicular to the solar surface). The flaring arch is associated with two small flares seen in the northern part of the AR close to the injection of material into the arch. During the evolution of the small flares a slight increase of the X-ray emission (precursor of the main flare) was recorded by GOES-7 at around 07:40 UT (cf., Figure 3(a)).

2.1.2. *Impulsive Phase*

The impulsive phase of the 3B/X12 flare began at 08:10 UT according to Hα observations (SHT and LC) and at 08:09 UT in X-rays. From the beginning of this large flare one can distinguish in the AR at least five flare ribbons. One of these ribbons that developed along an existing filament was very bright and even seen in the photographs taken through a wide-band 3Å Hα filter. Several minutes later, 08:16–08:19 UT, a part of the main ribbon covering one of the AR spots was observed in white light by Babin and Koval (1992, 1993), Battiola (1992) and in the Debrecen/Gyula Observatory (Kalmán, 1992; Schmieder *et al.*, 1994). At around 08:13 UT one segment of the main ribbon erupted in the shape of an arch. The arch, when observed through the wide-band 3Å filter, was as bright as the flare ribbons. Concurrent with the eruption of the flare arch, a surge was ejected from one of its

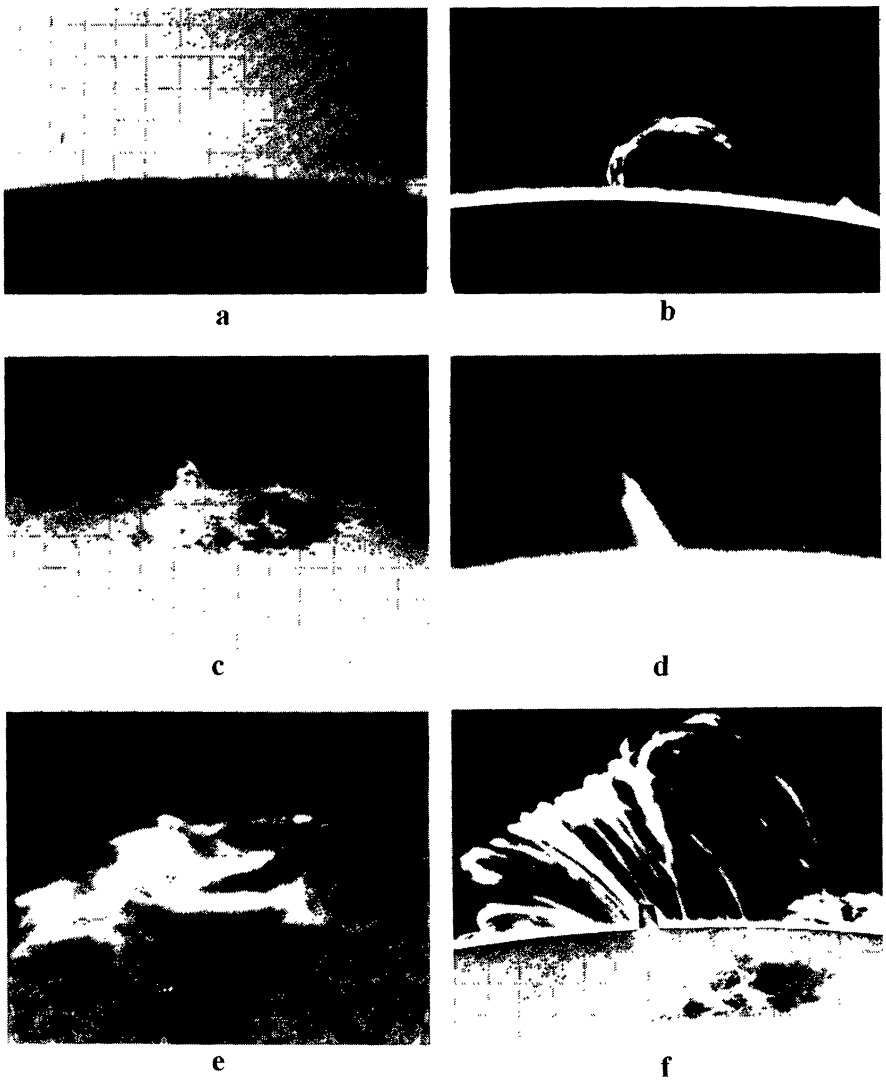

Fig. 2. Hα observations of the pre-flare flaring arch, surge and post-flare loop arcade: (a) the initial phase of evolution of the flaring arch at 07:41 UT (SC); (b) high-resolution picture of the flaring arch at 07:50 UT (LC); notice the fine filamentary structure of the arch; (c) eruption of an arch-shaped segment of the main flare ribbon and an initial phase of the surge eruption at 08:20 UT (LC); (d) the surge at a later phase of eruption at 08:26 UT (SHT); (e) the initial phase of the post-flare loop formation at 08:49 UT (SHT); (f) well-developed post-flare loop arcade at 12:08 UT (LC).

legs (see Figures 2(c) and 2(d)). The surge was ejected with an initial velocity of 80 km s^{-1} and was observed in Hα up to a projected height of 80 000 km above the ribbon. The system of ribbons inside the AR exhibited a flare-like brightness up to 10:30 UT (CH). In the meantime, the flare emission moved outside the AR towards the north.

We would like to stress here that very likely a CME should have been generated sometimes at the beginning of this complex flare. There are at least two reasons supporting such a supposition. The first one is that just at the impulsive phase of the flare one segment of the main ribbon of the flare erupted in the shape of an arch. Such eruptions, as well as the eruptions of the quiescent and active region prominences,

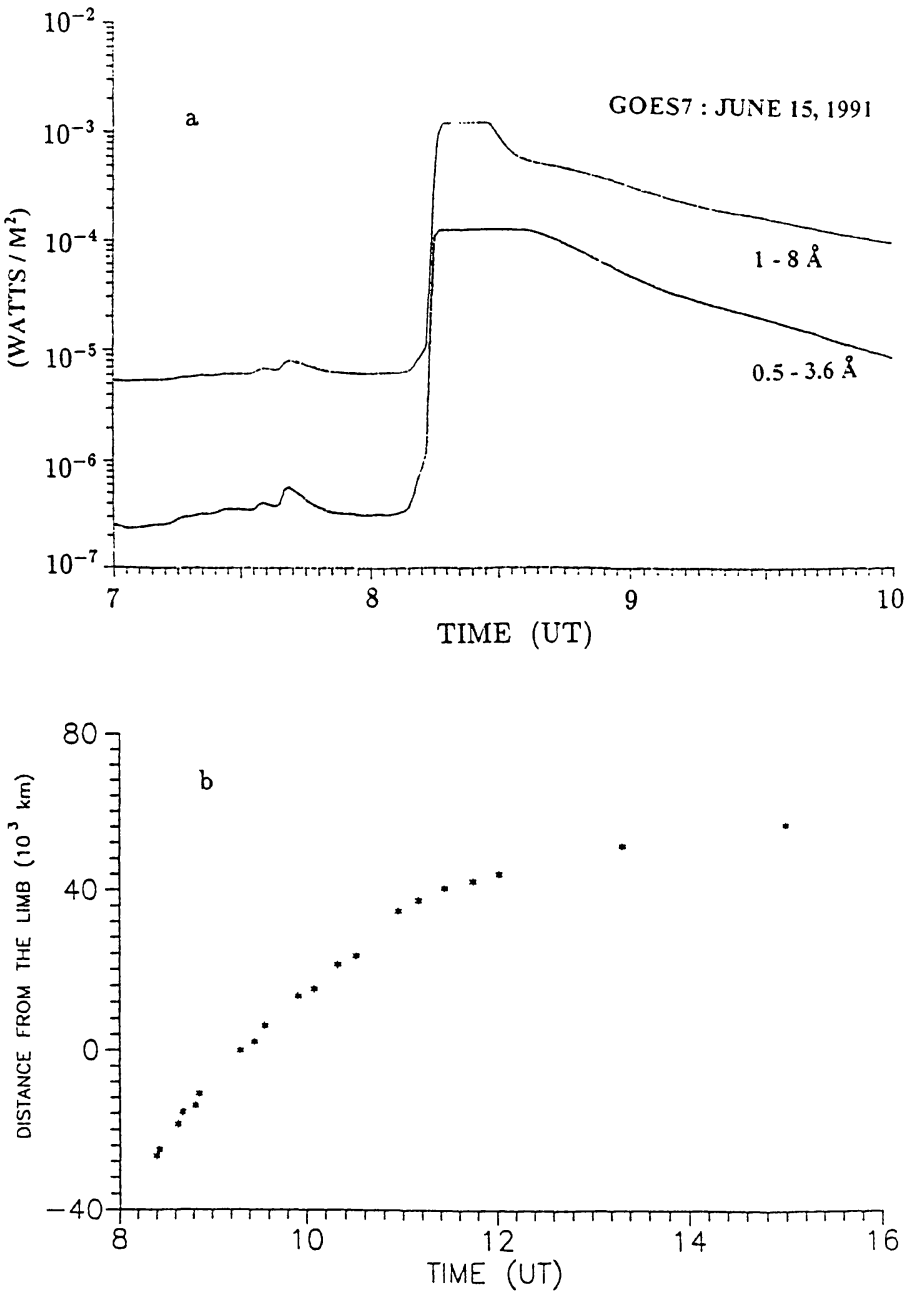

Fig. 3. (a) Time-profile of the GOES-7 soft X-ray burst; (b) time-altitude diagram of the post-flare loop arcade evolution.

are caused by eruptions of the associated huge magnetic systems (HMSs), which nearly simultaneously generate CMEs (Rompolt, 1984, 1990). The second one is that a number of X-ray bursts associated with flares and CMEs, investigated by Harrison *et al.* (1985), possessed an X-ray precursor. Such a precursor was also present in this flare.

2.1.3. *Post-Flare Loop Formation Phase*

Between two main ribbons of the flare a huge post-flare loop (PFL) system developed. The first manifestation of the PFL formation was the appearance of a bright, small compact loop evidently linking the two main ribbons at 08:22 UT. Above the ribbons one can recognize a diffusive cloud-like structure that very likely contains material from which other loops were formed later. A system of initially small PFL linking two main flare ribbons was clearly seen at 08:49 UT (SHT) (see Figure 2(e)). The continuously growing PFL system was observed up to 15:31 UT. It was observed in Hα for about 7 hours. The highest loop in the system attained a height of about 125 000 km above the AR at 12:08 UT and a height of 140 000 km at the end of the Wrocław observations (14:48 UT). A time–altitude diagram, made on the basis of the observations with SHT and CH, shows the evolution of a group of loops forming the middle part of the arcade, visible from the beginning up to the end of observations (Figure 3(b)). The maximum development of the PFL, taking into account the height, brightness and number of loops, took place at around 12:00 UT (cf., Figure 2(f)). On the following day we observed above the same AR material flowing down along the legs of several loops in the corona. We believe that these loops represent the final phase of evolution of the PFL system observed a day earlier. If so, the total time of Hα visibility of the PFL system was at least 24 hours! Simultaneously with the start of the impulsive phase of the flare and with the development of the long-duration PFL system, GOES-7 recorded a long-lasting X-ray burst (see Figure 3(a)). The X-ray emission in two energy channels of the GOES-7 started at 08:09 UT and lasted at least up to 20:00 UT, at which point it returned to its original level.

2.2. Radio Emission

For the present analysis we use data obtained with the fixed-frequency radiometers of IAP (Bern) and IZMIRAN (Troitsk) at 8 frequencies in the range of 3–50 GHz and with the sweep frequency radio spectrograph of Ondřejov Observatory in the 100–1200 MHz range, as well as some other observations.

2.2.1. *Microwave Emission*

At centimeter and millimeter wavelengths, the three flare phases mentioned above are clearly evident. According to *Solar-Geophysical Data* (1991), a weak (18–40 s.f.u.) simple burst near 07:38–07:45 UT was observed in the centimeter range (6–17 GHz), coinciding with the preflare heating phase and soft X-ray precursor. As Figure 4 shows, the microwave (3 GHz) burst itself has a complex non-monotonic time profile which is very similar to that of the June 3, 1982 flare (see Figure 1). The first component, corresponding to the main flare phase and eruption of the large surge, is a strong quasi-impulsive burst with a peak flux density of over 2×10^4 s.f.u. at 08:17 UT, with sharp decay of the flux density, and with a total duration of about 7 min.

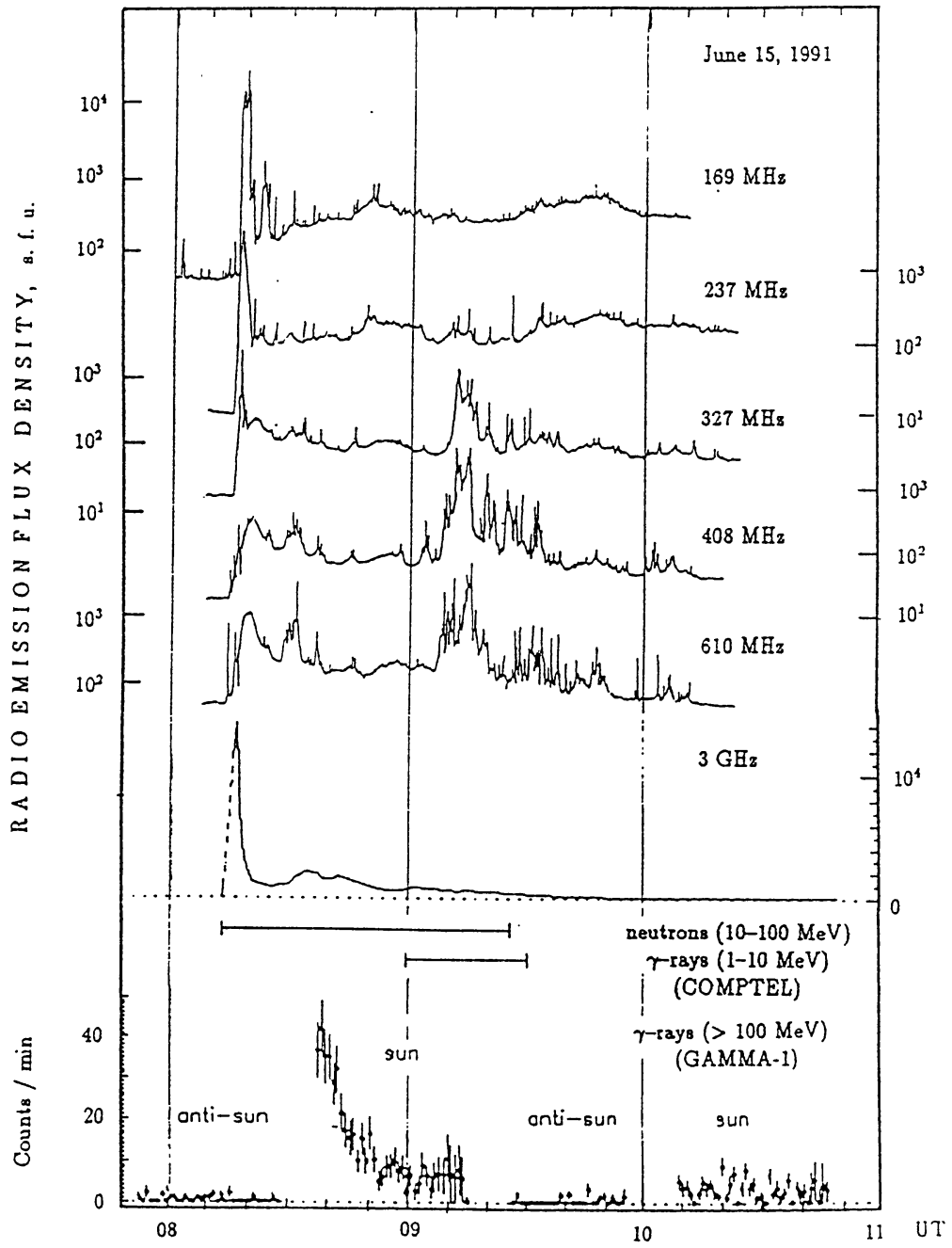

Fig. 4. A sketch of time profiles of the high-energy gamma-ray emission, total radio flux density at 169 and 3000 MHz by data of IZMIRAN, and flux density in right-hand circular polarization at 237, 327, 408, 610 MHz by measurements at the Trieste Astronomical Observatory. The production time of the 10–100 MeV neutrons, calculated by Debrunner *et al.* (1993) from the COMPTEL data, and observational time of the 1–10 MeV gamma-rays (Ryan *et al.*, 1993) are shown by horizontal bars in a lower panel.

Then, after some interval when the flux density decreases to the level of 750–1200 s.f.u., the second component starts to increase at 08:25–08:26 UT. It is important that the onset of this long-duration, post-burst enhancement coincides with beginning of the post-flare loop formation phase observed optically.

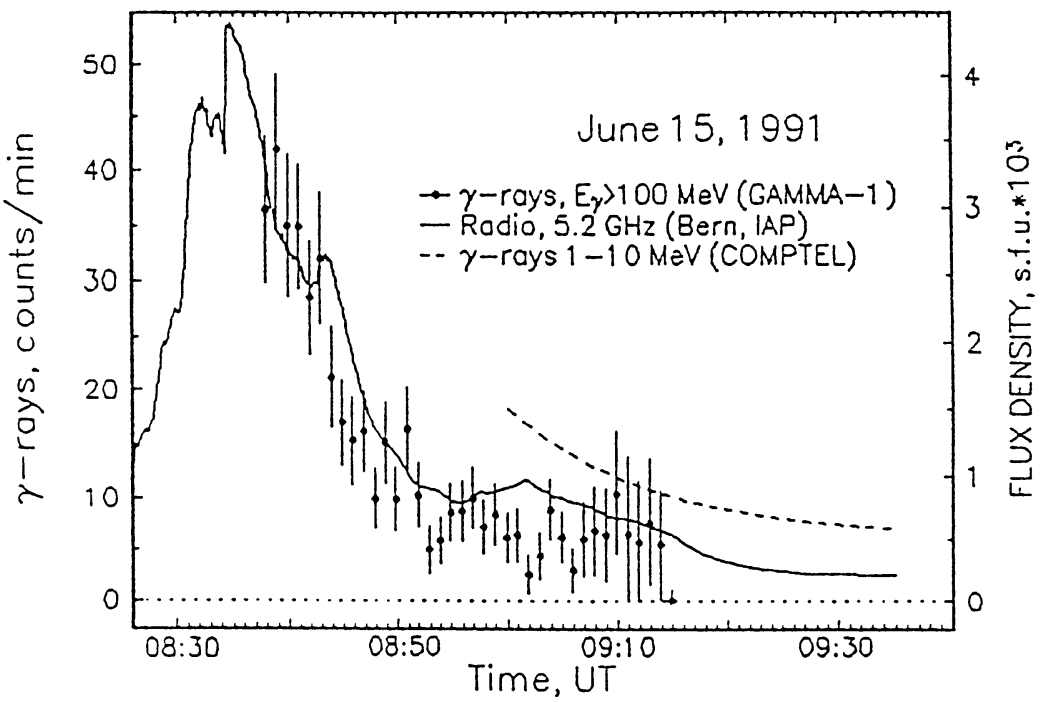

Fig. 5. Enlarged gamma-ray and microwave time profiles of the delayed component.

At 3–5 GHz, the main part of this radio component continues to decay until ~09:30 UT, but the flux density remains above the pre-burst background until 13–14 UT. The delayed component is much weaker than the impulsive burst, but its absolute intensity at 5.2 GHz is quite large, up to several thousands of s.f.u. (see below).

The large-scale picture of the delayed component shown in Figure 5 reveals that the post-burst enhancement of radio emission has an unsmoothed profile, including a number of sub-bursts with a time scale of 100–200 s. Such a complex structure is indicative of the nonstationary energy release during the the post-flare loop formation phase of the flare.

Figure 6 illustrates frequency spectra of the radio emission. For the first (impulsive) component, the peak flux density spectrum for the 08:14–08:17 UT interval comes from data of the Learmonth Observatory (*Solar-Geophysical Data*, 1991). For the second (delayed) component, a number of momentary spectra have been determined from the Bern data in order to analyze their time evolution. The spectra of both components differ strongly from simple, for example, gyrosynchrotron spectra (Dulk and Marsh, 1982), which testifies either to the inhomogeneous structure of the radio source or to the complicated energy distributions of radiating electrons.

The impulsive component has a separate decimetric peak of $S \approx 3.9 \times 10^4$ s.f.u. at 1415 MHz. At frequencies between 2.7–8.8 GHz, the flux density remains roughly constant at $S \approx (1.7–1.9) \times 10^4$ s.f.u. and then grows up to $S \approx 2.5 \times 10^4$ s.f.u. at 15.4 GHz.

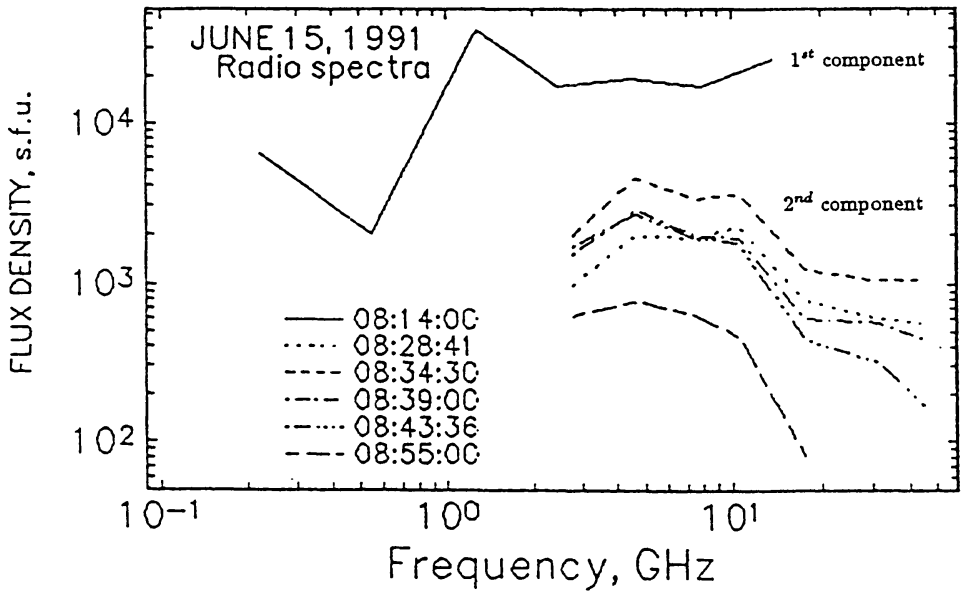

Fig. 6. The peak flux density spectrum of the impulsive microwave component at 08:14–08:17 UT by data of the Learmonth Observatory and some momentary spectra of the delayed component for 08:28:41–08:55 UT by measurements in Bern.

Unlike that, the second component at the moment of the peak intensity (08:34:40 UT) is characterized by a so-called soft radio spectrum with a maximum flux density of $S \approx 4.5 \times 10^3$ s.f.u. at 5.2 GHz. One more feature of this spectrum is its distinct high-frequency flattening at 19.6–50 GHz. Figure 6 shows also that the shape of the microwave spectrum, including the relatively low spectral maximum frequency, $f_m \approx 5.2$ GHz, and high-frequency flattening, remains practically the same during the main part of the second component. Only near the onset of this component at 08:28–08:33 UT, does the spectrum peak at 11.8 GHz with approximately equal flux densities at 5.2 and 11.8 GHz. As a whole, the evolution of the radio spectra during the extended component reduces to relative decrease of the flux density at high frequencies and increase at low frequencies. The similar frequency spectra throughout the delayed component indicate that the generation of the successive sub-bursts is mainly caused by the appearance of additional accelerated particles rather than by variations of other parameters of the radio sources such as the magnetic field strength.

It is important for the present study that as a whole the second microwave component of the flare under consideration by its observational features can be identified in particular with so-called extended or delayed microwave bursts (Cliver *et al.*, 1986; Kai *et al.*, 1986; Švestka, 1989). According to these studies, such events are closely associated with coronal mass ejections and interpreted as a result of a prolonged post-eruptive coronal particle acceleration via magnetic reconnection in post-flare loop system formation.

2.2.2. *Decimetric and Metric Bursts*

Analysis of the dynamic spectra shows that in the decimetric/metric range the flare radio emission is a complicated overlap of a slow-drifting, multi-band type II burst and intense continuous type IV burst with a rich fine structure. Let us consider only three features that are important for this study.

Firstly, the flare starts at 08:13:33-08:14:00 UT with several weak dm spikes in the range of 900–1000 MHz (see Figure 4). They are short-duration ($t \leq 0.1$ s) and narrowband ($\Delta f \approx 10$ MHz) bursts that are believed to be a manifestation of elementary 'quanta' of particle acceleration in the region of the flare energy release (see, e.g., Güdel, Ashwanden, and Benz, 1991). An upper limit on the background electron density in the acceleration source is obtained from the condition that the electromagnetic wave frequency must exceed the plasma frequency. This yields the value of $n_e \approx (1\text{–}1.2) \times 10^{10}$ cm^{-3}.

Secondly, the spikes mentioned above are followed by a group of type U bursts (Figure 7(a)) which drift slowly toward low frequencies: the top of the U bursts moves from 510 MHz at 08:14:46 UT to 300 MHz at 08:16:27 UT. This global negative drift is typical of the initial phase of the eruptive flares (Karlický, 1992) and can be explained by the propagation of electron beams in expanding magnetic loops. The electron density in such expanding loops is decreasing, which is why the U bursts are observed at lower frequencies. Taking into account the characteristic density height scale of 10^5 km for the coronal temperature of $T \approx 2 \times 10^6$ K, we can estimate the height difference between the top of the U bursts as 8×10^4 km and also the expanding loop velocity as 800 km s^{-1}. Moreover, during the impulsive phase at 08:16:00–08:18:40 UT, broadband pulsations with a characteristic period of 0.5 s were observed also in the 500–1200 MHz range.

Thirdly, in the post-flare loop formation phase, the prolonged decimetric/metric radio continuum with numerous variations and bursts of different intensity and time scale, including a number of reactivations and various fine structures, take place as well (see Figure 4). In particular, during the rise and peak of the delayed microwave component (08:29:00–08:32:10 UT) one more strong group of narrowband dm-spikes was fixed at 300–1000 MHz (Figure 7(b)). Their parameters, i.e., the duration and frequency width, were 0.1 s and 2–15 MHz, respectively. After this first reactivation, the second, stronger and prolonged one follows at 09:00–09:50 UT, which is especially intense at decimetric wavelengths and is accompanied by subsecond pulsations (09:06:55–09:37:00 UT, 300–900 MHz, and 09:30:30–09:32:00 UT, 100–400 MHz) as well as by fiber bursts (09:13:40 –09:18:30 UT, 500–900 MHz, and 09:35:10–09:35:13 UT, 400–500 MHz) (Figure 7(c)). The presence of these variations and fine structures, especially of dm-spikes, shows that the electron acceleration occurs also at the late phase of the flare. The displacement of the low-frequency boundary of the dm-spike emission to lower frequencies in comparison with the impulsive phase is indicative of higher altitude particle acceleration during the post-flare loop formation phase.

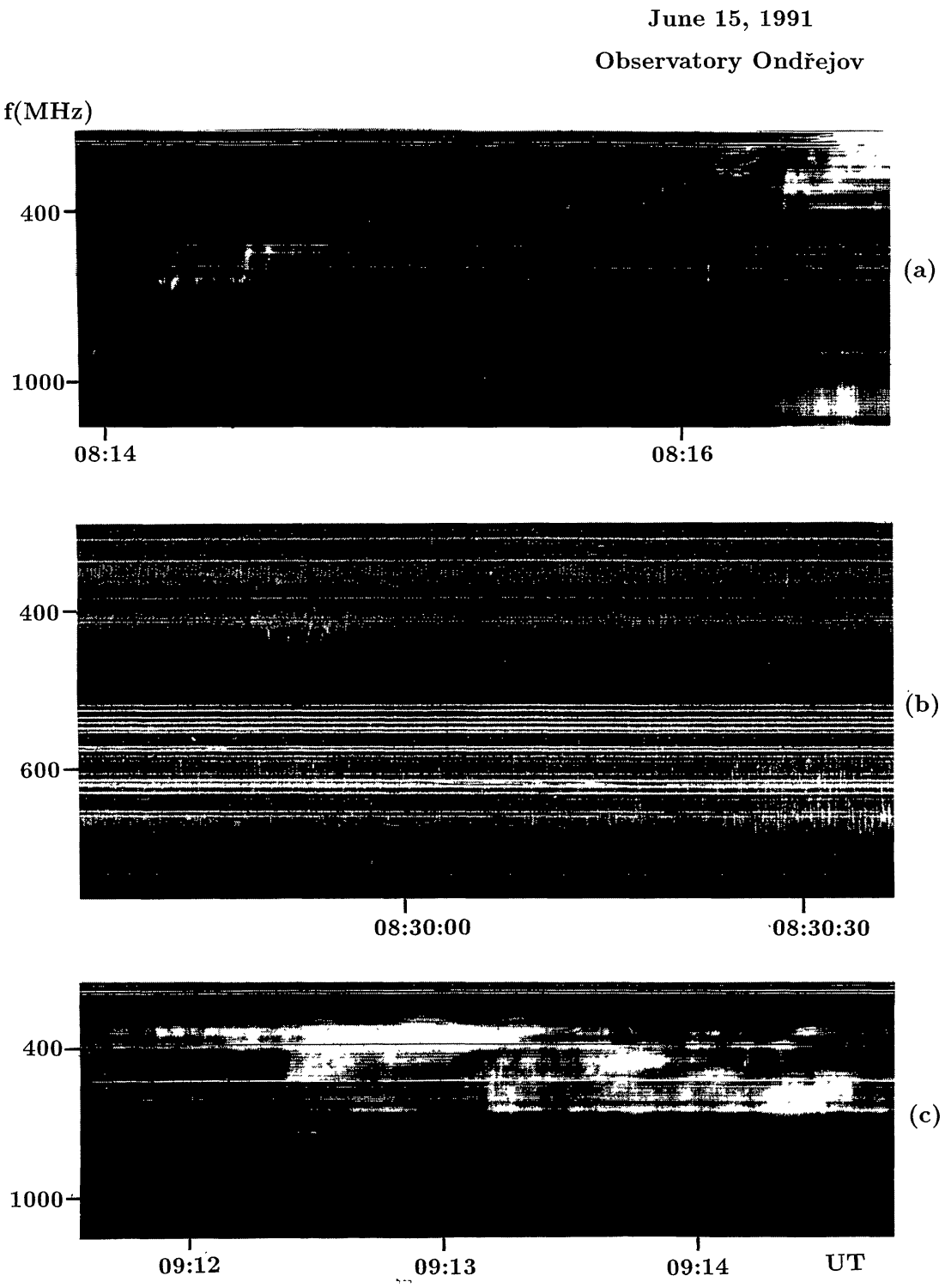

Fig. 7. Fragments of the Ondřejov dynamic radio spectrum: (a) a group of type U bursts at the start of the flare; (b) numerous narrowband dm spikes during the post-flare loop formation phase; (c) the second reactivation with fine structures.

It should be noted that the association of similar strongly variable radio emission and fine structures with the reactivation process in the post-flare loop phase connected with interactions of the loops was pointed out also for other large flares, such as the April 27, 1981 and June 3, 1982 events (Karlický, Aurass, and Mann, 1986; Zhang He-Qi and Chupp, 1989; Karlický and Zhou Ai-hua, 1993).

2.3. GAMMA-RAYS

2.3.1. *Time History*

The time profile of the June 15 flare in gamma-rays above 100 MeV registered by the GAMMA-1 telescope (Akimov *et al.*, 1988a) is displayed in Figure 4. During the solar observations an orbital period (92 min) was shared between solar and anti-solar orientations separated by the intervals of satellite slew when the telescope was off. GAMMA-1, being in shadow, could not register the impulsive phase and was switched on in solar attitude at 08:37:22 UT, just at the maximum of the delayed radio component. From 09:00:14 to 09:14:44 UT the satellite was traversing the South Atlantic Anomaly. For this interval we can not exclude the possibility of unexpected background variations. During the next orbit the high-energy gamma-ray flux was still well above the background. Then the telescope was switched off for technical reasons for a few days. An enlarged picture of the high energy gamma-radiation time history superimposed on the 5.2 GHz microwave delayed component is shown in Figure 5. The dashed line represents the characteristic decay time (13.9 min) of the 1–10 MeV gamma-ray emission during the COMPTEL/CGRO measurements at 08:59–09:37 UT (Ryan *et al.*, 1993).

One should note a similarity between the general trends (and perhaps some details) of the high-energy gamma-ray and microwave time profiles at the decay stage of the delayed component at 08:37–09:00 UT. One can see that at the adjoining time interval, where the COMPTEL data are available, the decays of gamma-ray and radio emissions are similar.

The general similarity of the gamma-ray and microwave emission appears to be maintained on a broader time scale as well. At least, the >100 MeV gamma-ray flux during the second GAMMA-1 orbit (after 10:08 UT) decreased by a factor of 4 in comparison with that at the end the first orbit, while for the radio flux density at 3–5.2 GHz, the corresponding factor is 5.

2.3.2. *Spectral Analysis*

At low energies, the sensitivity of GAMMA-1 varies significantly within the width of the energy response function. Therefore the calorimeter data do not directly reveal the real spectrum shape, so the application of some deconvolution procedure is necessary.

The unknown source spectrum is connected with the observed numbers of counts, N, in an arbitrary binned space of measured energies through the instrumental convolution function C(E). Its essential components – effective area and

energy-spread-function – were obtained by combination of calibration on an accelerator and Monte-Carlo calculations (Akimov *et al.*, 1988b).

The maximum likelihood method was applied with the use of the Poisson logarithmic likelihood function $L(\mathbf{N}, \boldsymbol{\mu})$, where the mean value $\boldsymbol{\mu}$ is a prediction from the energy spectrum model $F(E)$:

$$\boldsymbol{\mu} = \mathbf{b} + \int_E F(E)\mathbf{C}(E)\,\mathrm{d}E\,, \tag{1}$$

where $\mathbf{b}$ is the background expectation. $L(\mathbf{N}, \boldsymbol{\mu})$ must be maximized over the spectrum model parameters.

For the first orbit, only the 23-min period from the start of the solar observation to the anomaly entrance was used for the spectral analysis. As a first step we introduced a simple power-law spectrum model. This model turned out to be incompatible with the data.

In order to get a hint of the kind of spectrum model which would be the most adequate to the data, the maximum entropy deconvolution algorithm was applied (Cornwel and Evans, 1985). The power-law model was taken here as a 'background level' corresponding to zero information content. The maximum entropy nonparametric solution showed that the only spectral feature that can be supported by the data is a spectrum bend near 100 MeV. As the next step of our analysis, we examined a model

$$F(E) = AE^{-\gamma_1}[1 + (E/E_0)^2]^{(\gamma_1-\gamma_2)/2} \tag{2}$$

that corresponds to a double power-law spectrum with a smooth break at $E = E_0$ and exponents γ_1 at low and γ_2 at high energies.

Though the solution is not too sensitive to the value of E_0, formally the best fit was reached with $E_0 = 70$ MeV. Figure 8(a) displays the best fit with model (2) ($\gamma_1 = 6.3 \pm 1.4$, $\gamma_2 = 3.64 \pm 0.24$). The shaded area corresponds to a 68%-confidence region of possible solutions obtained by multiple repetition of the maximization routine with bootstrap samples extracted from the original data set. The shape of the spectrum with a maximum at 70–100 MeV indicates that most of the photons originated from neutral pion decay.

In a search for spectral variation, the total 23-min period was divided into three consecutive time intervals of duration 5, 8, and 10 min, containing equal total numbers of photons. In general, the spectrum shape was found to be stable, but values of the exponent at high energies (γ_2) showed a tendency to soften: the first interval 3.13 ± 0.37, the second 3.75 ± 0.55, the third 4.31 ± 0.57.

We are confident that the spectrum reconstruction procedure applied together with the telescope characteristics used does not suffer from any systematic error which could result in an artificial spectrum bend at low energies. This is verified by several measurements during the GAMMA-1 flight, e.g., in a very short impulsive

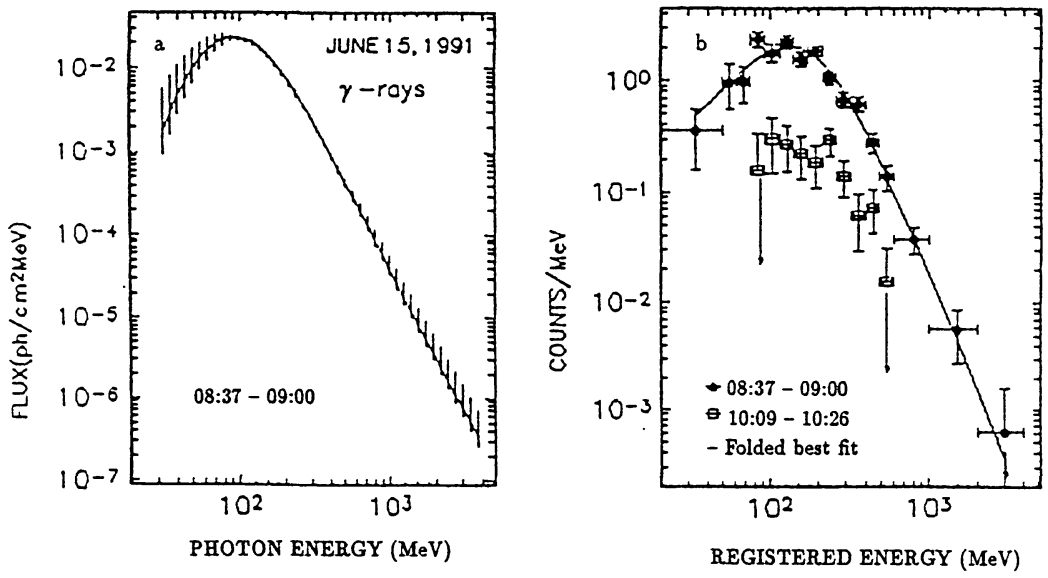

Fig. 8. The gamma-ray energy spectrum in the first orbit (a) and energy distribution of counts in the first and second orbits (b).

gamma-ray flare on March 26, 1991 (rise time ~1 s) a pure power-law spectrum, evidently of the electron bremsstrahlung origin, was obtained (Akimov *et al.*, 1994b); observation of atmospheric gamma-radiation from the Earth's limb gave also a power-law spectrum. It should be added that telescope characteristics were being monitored in flight by a rich set of housekeeping data and daily calibrations and showed very high stability (Akimov *et al.*, 1991). Minor corrections were introduced when necessary. The energy spectrum and average intensity of the instrumental background were also stable during the flight.

The curve in Figure 8(b) represents the photon spectrum from Figure 8(a) folded with the energy dependence of the telescope effective area and energy response function. It demonstrates a good agreement with the registered counts (filled circles). Open squares show the counts in the second orbit. Scarce statistics do not allow one to construct a reliable photon spectrum, but the general similarity of data from the two orbits indicates that the photon spectrum did not change significantly in 1.5 hour.

The COMPTEL/CGRO registered gamma-ray emission from this flare (Ryan *et al.*, 1993) in the energy range 1–10 MeV during the time interval 08:59–09:37 UT (see Figure 4). The gamma-ray spectrum contained definitely the 2.2 MeV neutron capture line, a broad feature at 4.4 MeV, and probably some lines below 2 MeV, indicating the presence of protons with energies of tens of MeV.

2.4. Cosmic Rays

In this subsection we analyze possible relation between the energetic particles which produce various emissions on the Sun and those observed at the orbit of the Earth. The increase of solar cosmic rays generated by this flare was observed by

practically all the detectors aboard the spacecraft operated at that time. On the Earth the increase was detected by most of the neutron monitors with geomagnetic cut-off rigidities <7 GV. Besides, the COMPTEL telescope aboard the CGRO satellite registered a flux of solar neutrons in the 10–100 MeV energy range (Debrunner *et al.*, 1993). The ground level enhancement (GLE) of the cosmic rays was almost isotropic from the very onset, which is unusual for events caused by western flares. This fact, noticed already in the first studies of this flare (Smart and Shea, 1993; Akimov *et al.*, 1993), makes the analysis of the proton increase much easier. In particular, simple isotropic diffusion models can be applied for description of the energetic particle propagation and features of the proton increase.

Data from 16 different channels of the GOES-6 and -7 (NGDC CD, 1994) and IMP-8 (Armstrong, 1993) satellites and of 28 neutron monitors (*GLE Data Base*, 1994) allowed us to derive time and energy dependencies of the differential proton fluxes near the Earth using the special method elaborated by Belov and Eroshenko (1995). For the proton event under consideration, the differential proton fluxes near the Earth have been found for each 5-min interval from the onset to the very end of the increase in the 10 MeV–10 GeV energy range. This sufficiently detailed time-energy picture allows us to investigate the main properties of the increase.

If the proton emission from the Sun starts at a moment t_0, lasts during a time interval Δt, and is described by a function $f(\tau)$, then in the framework of an isotropic diffusion model, an equation for the proton flux observed near the Earth at the moment t is

$$I(t) = A \int_{t_0}^{t_0+\Delta t} f(\tau) \exp\left(\frac{b}{t-\tau}\right) (t-\tau)^{\gamma} \, \mathrm{d}\tau \, . \tag{3}$$

The parameters A, γ, b in this equation depend on the diffusion characteristics in interplanetary space and on the particle energy. They should be found for different energies by a least-square method.

A number of the simple 2–3 parameter forms were tested for $f(\tau)$. The best agreement with experimental data was obtained for the simplest rectangular form. In this case the residual dispersion decreases by 3–6 times relative to the instantaneous emission model. Analysis of the modeling results obtained revealed some essential differences between the ejection time of low- and high-energy protons. The 175–350 MeV protons appeared to be ejected from 08:23 ± 00:01 UT during 6 ± 1 min (in photon arrival time). This time interval coincides approximately with the onset of the post-flare loop formation phase observed in the optical range and with the onset of the delayed microwave component. The ejection of high-energy protons (1300–4000 MeV) occurred approximately at the same time (08:26 ± 0:03 UT), but it could have had a shorter duration.

For low-energy ($E < 80$ MeV) protons, reliable data on the emission duration could not be obtained, but in any case a beginning of the low-energy proton ejection could not be much delayed relative to the onset of the impulsive phase of the flare.

This statement is supported by optical observations (Babin and Koval, 1993) and analysis (Belov, Eroshenko, and Lifschits, 1994) of the white-light flare as well as by the neutron observations (Debrunner *et al.*, 1993). The white-light emission, that is believed to be initiated by the <100 MeV protons, started before 08:15 UT and lasted up to 08:23 UT. The low-energy neutrons also were ejected just at the beginning of the impulsive phase of the flare. At the same time, the lack of >100 MeV protons till 08:23 UT explains why at the onset of the flare (08:13–08:23 UT) only the ejection of the low-energy neutrons was observed.

As a next step it is reasonable to use the shape of the microwave burst as the profile of the proton ejection. Figure 9 shows results of calculations of time profiles for two proton energies in the cases when the whole microwave (19.6 GHz) time profile (top panel) and only its delayed component (bottom panel) were taken as an ejection function $f(\tau)$. One can see that in the former variant the model calculations lead to too early an onset and too slow an increase of the proton flux at high energies. The latter variant gives much better agreement with the experimental data, particularly for high-energy protons.

The results outlined above provide evidence that emission of low-energy protons embraced both the impulsive and the delayed phases of the flare, while the main part of the >100 MeV protons was ejected after the end of the impulsive phase. Other evidence in favour of this conclusion can be inferred from the analysis of the energy spectrum variations at the event onset. Figure 10 illustrates the proton energy spectra for the initial stage of the proton increase. Usually proton spectra before the event maximum are harder than in the maximum itself (the spectrum in the maximum is also shown in Figure 10) and after the maximum the slope of the spectrum becomes steeper. In this event, such behavior is observed only from the third 5-min interval (08:40–08:45 UT) but during the first 10 min (08:30–08:40 UT) the proton spectrum has an unusual shape with a pronounced maximum at 200–300 MeV. This can take place only under prolonged proton emission with a hardening of the energy spectrum.

3. Discussion

Thus the features of the radio bursts, high-energy gamma-ray emission, 0.8–8 MeV gamma-ray continuum and lines, cosmic rays, as well as the optical data described above are directly indicative of the presence of electrons with energies from some hundreds of keV to at least several MeV and protons with energies from some tens of MeV up to several GeV in the flare region during many tens of minutes at the post-flare loop formation phase.

3.1. Prolonged Acceleration Rather than Trapping

As we wrote in Section 1, there are two possibilities to explain the presence of the energetic particles at the late stage of the flare:

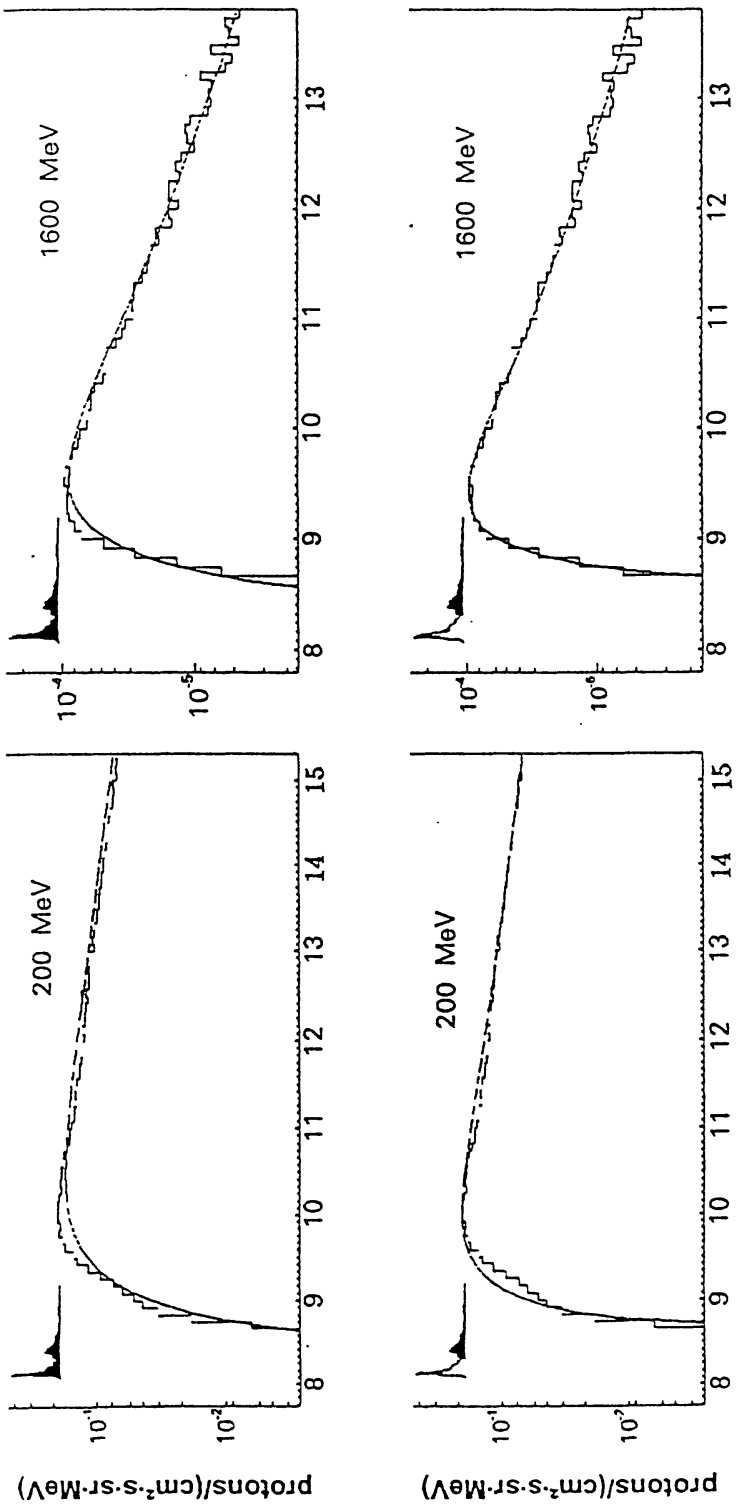

Fig. 9. Comparison of the observed and calculated differential profiles of the 200 and 1600 MeV protons for the ejection functions identified with the whole profile of the microwave burst (upper row) and of the delayed microwave component only (lower row), as shown by the inserted fragments.

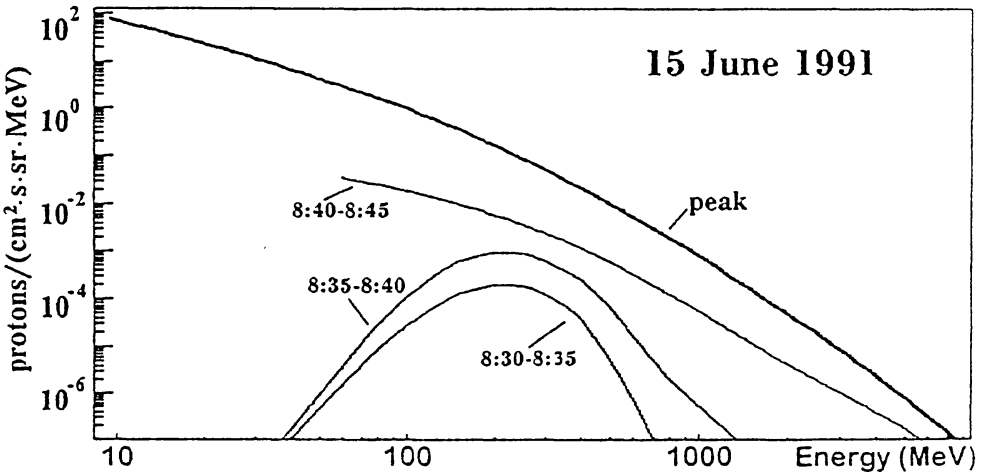

Fig. 10. Differential proton spectra of cosmic rays near the Earth, observed during the three first five-min intervals after the onset, and the peak proton spectrum for the June 15, 1991 event.

(a) The comparatively short acceleration of particles in the impulsive phase of the flare followed by their long trapping in the coronal magnetic loops and slow precipitation into denser footpoint regions.

(b) The continuous particle acceleration during the late phase of the flare.

Mandzhavidze *et al.* (1993) combined the GAMMA-1 and COMPTEL/CGRO gamma-ray data for the June 15, 1991 flare and showed that it is possible to account for these observations by assuming that after an impulsive acceleration particles were trapped in magnetic loops provided the plasma density was low at the trap location, the plasma turbulence level was decreasing during the late phase of the flare, and a gradient drift of particles from coronal loops was suppressed by twist of the loop magnetic lines (Yun-Tung Lau, Northrop, and Finn, 1993).

We believe that the complex of the observational data presented in Section 2 bear some evidence of prolonged particle acceleration during the late phase of the flare rather than of the long-term trapping of energetic electrons and ions accelerated in the impulsive phase. The main arguments are the following:

(1) *Variability of the microwave time profiles.* The microwave emission flux in the delayed phase of the flare varies significantly with a characteristic time of 100–200 s. If these variations were caused by fast changes of the magnetic field strength or plasma density, it would result in variations of the spectral maximum frequency or the degree of the frequency spectrum suppression at low frequencies. An analysis of the observed frequency spectrum testifies to an absence of these effects. Consequently, we have to ascribe the microwave sub-bursts to additional electron acceleration acting during the post-flare loop formation phase.

(2) *Variability and fine structure of the decimetric/metric bursts.* The strong variability reactivations and numerous radio bursts observed during the late phase of the flare can hardly be explained by phenomena other than an additional acceleration of keV electrons. At the same time, the fine structures, especially such as the dm-spikes, appear to be an independent indicator of the electron acceleration

in this phase of the flare, in particular, of elementary events of the acceleration. It is important to be reminded of the conclusion of Subsection 2.2.2, that according to the observed frequencies of the dm-spikes, the source of particle acceleration was situated higher in the corona in the late phase than in the impulsive phase of the flare.

(3) *Similarity of the microwave and gamma-ray time profiles in the delayed phase.* It is difficult to account for the observed similarity between profiles of the delayed component of the microwave burst, 1–10 MeV and 30 MeV–2 GeV gamma-ray emissions by the long capture of such different kinds of particles as the hundreds of keV and some MeV electrons, and tens of MeV and GeV protons. In the weak diffusion regime, when the lifetime of particles is a maximum and determined by Coulomb collisions, the 1 GeV protons live in the trap some thousands of times longer than >500 keV electrons. If following, for example, Mandzhavidze and Ramaty (1992a) one accepts the value $n \approx 10^{10}$ cm^{-3} for the background plasma density, then without taking into account the gradient drift, the 1 GeV protons can live in the trap for about 2×10^5 s, but the lifetime of the 500 keV electrons at the same density is restricted to 30 s. The precipitation of such different particles into the loss-cone by scattering due to plasma turbulence also cannot occur at the same rate. Therefore the observed similarity of the profiles is due to a long-term nonstationary acceleration rather than a capture of particles in the trap.

(4) *Long-lasting escape of the accelerated particles into interplanetary space.* The peculiarities of the cosmic ray increase outlined in Section 2.4 give us grounds to reject the simplest model of instantaneous and simultaneous ejection of protons of all energies. The model of the long ejection matches the experimental data better. The composition of all the results obtained reveals that protons of relatively low energies (<80 MeV) were being ejected, beginning from the impulsive phase of the flare, but the high-energy protons (>150 MeV) were generated after the end of the impulsive phase, and the beginning of their ejection approximately coincided with the onset of the post-flare loop formation phase and the delayed microwave component. As a whole, the close relation between the characteristics of the energetic particles observed as cosmic rays and that producing the microwave and gamma-ray emissions appears to show that these two particle populations had a common origin and were accelerated on the Sun.

It should be added that, as Debrunner *et al.* (1993) concluded from the analysis of the COMPTEL data, the generation of neutrons started at the onset of the impulsive phase and lasted for over one hour with the higher-energy neutrons being produced later than lower-energy ones.

3.2. POST-ERUPTION ENERGY RELEASE AS A SOURCE OF THE PROLONGED PARTICLE ACCELERATION

Thus, we believe that the long-duration gamma-ray emission and the delayed radio bursts in this flare stemmed from ions and electrons accelerated during the late phase of the flare.

If the variant of the prolonged particle acceleration is correct, then one of the causes of such an acceleration could be, in principle, a coronal shock wave generating a type II radio burst (see, e.g., Ramaty *et al.*, 1987). However, such a shock acceleration appears to be not suitable for the interpretation of the delayed component of the gamma-ray and microwave emission. The most obvious reason is that at the time of the delayed component the shock propagates already at such a high altitude in the corona that the particles are not able to return to the chromosphere and to produce, in particular, the gamma-rays (Kahler, 1984; Mandzhavidze and Ramaty, 1992b). For example, one can see in Figure 1 that for the June 3, 1982 flare, at the moment of the delayed microwave component, the altitude of the front of the coronal mass ejection, which location is like that of the shock wave, is approximately 2.5 $R_{\odot}$ above the photosphere (Sheeley *et al.*, 1985). The analysis of the dynamic spectrum of the type II burst for the June 15, 1991 flare gives a close estimation of the shock wave altitude.

Besides the primary energy release in the impulsive phase and coronal shock wave, there is one more source of prolonged particle acceleration high in the corona which is connected with CMEs (see, for example, reviews by Švestka (1989), Kahler (1992), and Chertok (1993)). In the process of the CME eruption, the magnetic field is strongly disturbed in the extensive region of the corona. The helmet magnetic configurations with initially closed field lines in the low corona are stretched by the CME and are converted into mainly open structures. Then, in the post-eruptive phase, the magnetic field restores gradually to its initial state. The restoration happens via the magnetic reconnection in a coronal vertical current sheet and results in a prolonged particle acceleration.

The post-eruption energy release in large flares is considered as a possible source of prolonged acceleration of electrons with energies of tens–hundreds of keV, which are responsible in particular for long-duration hard X-ray and microwave bursts (Kopp and Pneuman, 1976; Anzer and Pneuman, 1982; Kahler, 1984; Cliver *et al.*, 1986; Kai *et al.*, 1986; Karlický, Aurass, and Mann, 1986; Martens and Kuin, 1989; Švestka, 1989). As far as a proton acceleration during the post-eruption phase is concerned, Bazilevskaya *et al.* (1990), analyzed observational data and argued that this process can produce 10–30 MeV protons observed sometimes in interplanetary space as so-called surplus proton fluxes.

Our present analysis provides some evidences that there are powerful eruptive flares in which the restoration of the coronal magnetic field after propagation of a large CME appears to be accompanied by a prolonged acceleration of both electrons and protons up to energies as high as some MeV and GeV, respectively.

Unfortunately, there were no white-light satellite observations of CMEs for this flare. However, there are some indirect data indicating a CME eruption as well as direct optical observations of the long post-flare loop formation phase and various radio manifestations of the post-eruption energy release in the flare. Among signs of the CME eruption we can point out, for example, is a coincidence of the brightening and development of the pre-flare loop with a soft X-ray precursor of the flare (Harrison *et al.*, 1985; Harrison and Sime, 1989); the presence of a number of eruptive events, including the surge and a loop-type eruptive prominence (Subsection 2.1); an association of the drifting group of U-type radio bursts in the initial phase of the flare with extending coronal loops (Subsection 2.2); an appearance of a large and long-existing post-flare loop system; and, lastly, an associated geomagnetic storm with a sudden commencement on June 17 at 10:19 UT (*Solar-Geophysical Data*, 1991) corresponding to an average velocity of the disturbance on the Sun–Earth route of about 830 km s^{-1}.

As far as the post-eruption energy release is concerned, practically all the most typical attributes of this phase were present and well developed in this flare (Section 2). The most clear manifestation of this process is an evolving and large-scale post-flare loop system observed optically for at least 10 hours. It was accompanied also by the long-duration soft X-ray burst, delayed microwave component with a soft frequency spectrum, multi-hour decimetric/metric radio emission with numerous variations and fine structures, etc.

3.3. Particle Acceleration in a High Coronal Current Sheet

A reconnecting current sheet (RCS) forming behind a rising CME or loop prominence is a place where prolonged energy release occurs, mainly in the form of high-energy particles. The reason for this is a strong, direct electric field generated inside RCS, that efficiently accelerates charged particles (Somov, 1981). As RCS forms very high above the photosphere, the plasma density outside RCS is low and collisional energy losses can be ignored. This fact allows us to explain the efficient generation of relativistic particles in flares of the type considered (Litvinenko and Somov, 1995).

Some simple estimates confirm the above-mentioned scenario. A typical CME speed of upward motion equals the Alfvén speed in the corona $V_A \approx 1000$ km s^{-1}. A typical speed of plasma inflow into RCS v is an order of magnitude lower. Here we assurme a fast reconnection regime in the RCS. Such a regime is known to be realized in non-neutral sheets (see Somov, 1994, and references therein). Taking for illustrative purposes $v \approx 100$ km s^{-1} and a characteristic value of the magnetic field $B_0 \approx 100$ G near RCS, we obtain the direct electric field inside RCS,

$$E = \frac{1}{c} v B_0 \approx 10 \text{ V cm}^{-1} , \tag{4}$$

where c is the speed of light. Electric fields of this order are actually observed in active regions, in particular, in erupting prominences.

The maximum energy gain for a particle accelerated in RCS is determined by the potential drop along the sheet and equals

$$U = eEL \approx 100 \text{ GeV} \tag{5}$$

if $L \approx 10^{10}$ cm is a characteristic length of RCS. Clearly this value, U, is amply sufficient for the explanation of the extended acceleration phase, though taking care of the magnetic field in the RCS can diminish the actual maximum energy, $\mathcal{E}_{\max}$.

Speiser (1965) treated the particle acceleration in current sheets, taking into account both the reconnecting field and a small transverse (perpendicular to the RCS plane) magnetic field component $B_\perp = \xi_\perp B_0$. Litvinenko and Somov (1993) generalized the treatment by including into consideration the longitudinal magnetic field. This component efficiently magnetizes accelerated electrons in RCS, but cannot influence motion of relativistic protons and heavier ions that are of primary interest to us here. Hence, in the simplest approximation, we can use the basic Speiser result to estimate the energy gain, $\Delta\mathcal{E}$, for particles of mass m and charge e accelerated in the RCS:

$$\Delta\mathcal{E} = 2mc^2 \left(\frac{E}{B_\perp}\right)^2 . \tag{6}$$

Thus, on the one hand, electrons acquire relativistic energy in RCSs with a non-zero longitudinal field (Litvinenko and Somov, 1993). On the other hand, application of Equations (4) and (6) to the model of a high-temperature turbulent RCS (Somov, 1992), formed behind a rising CME, shows that a non-zero $B_\perp$ radically restricts the energy of heavier particles: $\mathcal{E}_{\max} \leq \Delta\mathcal{E} = 2m_p v^2 \xi_\perp^{-2}$ for protons cannot exceed 20 MeV if a typical value of $\xi_\perp \approx 3 \times 10^{-3}$ ($B_\perp \approx 0.3$ G) is assumed (see Section 3 in Litvinenko and Somov, 1995). Therefore, the relativistic energies cannot be reached after a single 'interaction' of the particle with the RCS in the framework of Speiser's model.

We suggest that charged particles interact with RCS more then once, each time gaining a finite, relatively small amount of energy. The cumulative effect could give the required relativistic acceleration. The factor that makes positively charged particles return to RCS is the transverse electric field directed toward the sheet (Litvinenko and Somov, 1995),

$$E_\perp = 2\pi\sigma^q , \tag{7}$$

where the magnitude of the electric charge density integrated over the sheet thickness is

$$\sigma^q = \left(\frac{u}{c}\right)^2 nea . \tag{8}$$

According to Litvinenko and Somov (1995), the maximum energy of protons is

$$\mathcal{E}_{\max} = \frac{\phi}{\xi_\perp^2}\left(1 + \sqrt{1 - \xi_\perp^2 + \frac{\xi_\perp^4 m^2 c^4}{\phi^2}}\right), \tag{9}$$

where $\phi \approx kT$. Formula (9) shows that protons can actually be accelerated to GeV energies in the high-temperature turbulent RCS: for instance, $\mathcal{E}_{\max} \approx 2.4$ GeV provided $T \approx 10^8$ K.

This result and very short acceleration time (see Equation (21) in Litvinenko and Somov, 1995) clearly demonstrate the possibility of an efficient acceleration of protons by a direct electric field, E, in a reconnecting current sheets during the late phases of solar flares.

4. Conclusion

Thus the main conclusion of this paper is that the long-duration and high-energy gamma-ray emission observed in the June 15, 1991 flare appears to be mainly a result of a continuous particle acceleration during the late phase of the flare, rather than a prolonged trapping of particles from the impulsive phase. This conclusion is based on the analysis of behavior of electrons and protons of different energies by means of the comparison of the gamma-ray emission with radio bursts and other accompanying phenomena.

Kocharov *et al.* (1994) came to a similar conclusion comparing mainly the energy spectra and the quantity of energetic particles which produced the gamma-ray emission with that observed near the Earth.

This conclusion seems to be correct, at least for the gamma-ray emission observed during the delayed microwave component. We do not exclude that at the very final stage of the flare the continuous acceleration is followed by a trapping of particles that provides the long gradual decay of the microwave and gamma-ray emissions.

We argue also that the most probable source of so long acceleration is a post-eruption energy release caused by a restoration of the coronal magnetic field after the CME eruption. The theoretical estimations also show that a large direct electric field inside a reconnecting current sheet, which is formed behind a rising CME, can result in acceleration of protons up to GeV energies. Our consideration reveals that the post-eruption energy release is a much more important process of the flare development than it was considered to be before. It is evident that the scenario suggested by us for the June 15, 1991 flare has a general character and can take place in other events.

For example, in another large flare of June 4, 1991, long-duration emissions of gamma-ray lines and high-energy neutrons with a clear two-component time

structure, corresponding to impulsive and delayed microwave components, were observed (see Struminsky, Matsuoka, and Takahashi, 1994, and references therein). The authors show that in this flare the second component of acceleration is also characterized by a much harder proton spectrum than the first one. Again, the similarity of gamma-ray, neutron, and microwave profiles means that effective particle acceleration occurred both in the impulsive and delayed phases.

In a recent paper Ramaty and Mandzhavidze (1994) reconsidered their previous conclusion concerning the origin of the long-duration gamma-ray emission in the June 11, 1991 flare. They noted that a clear similarity takes place between the time profiles of the 2.22 MeV gamma-ray line emission observed with COMPTEL and OSSE in the impulsive and delayed phases and the time history of the >50 MeV pion decay emission extended back to the impulsive phase. They estimated also that the magnetic field needed to allow trapping of the high-energy electrons responsible for the 50–70 MeV bremsstrahlung gamma-ray excess that is present for about 2 hours after the impulsive phase of the flare is inconsistent with the observed microwave flux. Therefore, Ramaty and Mandzhavidze (1994) came to the conclusion that during at least the first 3 hours after beginning of the flare, pure trapping of energetic particles cannot account for the observations and, consequently, prolonged multiple acceleration episodes are necessary (Chertok, 1995).

The existence of the well-developed post-flare loop systems in the flares on June 4 and 11, 1991 allows us to suppose that in these flare the acceleration in the delayed phase was also caused by the post-eruption energy release.

The two-stage energy release with harder gamma-ray spectrum in the delayed phase took place also in the much shorter and less powerful flare of March 26, 1991 (Akimov *et al.*, 1994b), although no pronounced CME was observed in this case. It means that second-stage acceleration may also occur when the preflare magnetic structures are disturbed not by a large CME, but by other factors such as rapidly expanding and evolving coronal loops.

Further experimental and theoretical investigations of many flares are necessary to study in detail features of the post-eruption energy release and the prolonged particle acceleration up to very high energies in the late stage of solar flares.

Acknowledgements

The authors are grateful to T. P. Armstrong for providing the IMP-8 cosmic-ray data. We are also indebted to P. Zlobec for supplying fixed-frequency radio data of the Trieste Astronomical Observatory. The Wrocław co-authors would like to thank the Polish Committee of Scientific Research for the support under Grant KBN No. 2 109 92 03. The work of A.V.B. and I.M.Ch. was supported in part by the Russian Federal Astronomical Program under Grant 4–129 and the Russian Foundation of Fundamental Research under Grants 93–02–02864, 94–02–03096,

and 95–02–06100a. I.M.Ch. acknowledges also support from the C&EE Program of the European Southern Observatory under Grant A-04–008. V.V.A and N.G.L. are grateful to the RFFR for support by Grant 94–02–03316-a. A.M. acknowledges the support by the Swiss National Science Foundation Grant 20–36417.92. We are grateful to an anonymous referee for helpful comments and suggestions, as well as for corrections of our English.

References

Akimov, V. V. and 75 co-authors: 1988a, *Space Sci. Rev.* **49**, 111.
Akimov, V. V. and 45 co-authors: 1988b, *Space Sci. Rev.* **49**, 125.
Akimov, V. V. and 20 co-authors: 1991, *22nd Int. Cosmic Ray Conf.* **2**, 483.
Akimov, V. V. and 32 co-authors: 1991, *22nd Int. Cosmic Ray Conf.* **3**, 73.
Akimov, V. V., Leikov, N. G., Belov, A. V., Chertok, I. M., Kurt, V. G., Magun, A., and Melnikov, V. F.: 1993, *23th Int. Cosmic Ray Conf.* **3**, 111.
Akimov, V. V., Leikov, N. G., Belov, A. V., Chertok, I. M., Kurt, V. G., Magun, A., and Melnikov, V. F.: 1994a, in J. M. Ryan and W. T. Vestrand (eds.), *AIP Conf. Proc. No. 294, High Energy Solar Phenomena: A New Era of Spacecraft Measurements*, AIP, New York, p. 106.
Akimov, V. V., Leikov, N. G., Kurt, V. G., and Chertok, I. M.: 1994b, in J. M. Ryan and W. T. Vestrand (eds.), *AIP Conf. Proc. No. 294, High Energy Solar Phenomena: A New Era of Spacecraft Measurements*, AIP, New York, p. 130.
Anzer, U. and Pneuman, G. W.: 1982, *Solar Phys.* **79**, 129.
Armstrong, T. P.: 1993, private communication.
Babin, A. N. and Koval, A. N.: 1992, *Pisma v Astron. Zh.* **18**, 727.
Babin, A. N. and Koval, A. N.: 1993, *Izv. Krymsk. Astrofiz. Obs.* **88**, 60.
Battiola, R.: 1992, private communication.
Bazilevskaya, G. A., Sladkova, A. I., Fomichev, V. V., and Chertok, I. M.: 1990, *Soviet Astron.* **34**, 205.
Belov, A. V. and Eroshenko, E. A.: 1995, *Adv. Space Res.* **17**, 167.
Belov, A. V., Eroshenko, E. A., and Lifshits, M. A.: 1994, *Proc. 8th STP Symp.*, Sendai, Japan, p. 26.
Chertok, I. M.: 1993, *Astron. Rep.* **90**, 135.
Chertok, I. M.: 1995, in T. Watanabe (ed.), *Proc. Second SOLTIP Symp.*, Nakaminato, Japan, in press.
Chupp, E. L. and Walker, A. B. C. (eds.): 1988, *The High-Energy Aspects of Solar Flares. Solar Phys.* **118**, 371 p.
Chupp, E. L., Forrest, D. J., Vestrand, W. T., Debrunner, H., Fluckiger, E., Cooper, J. F., Kanbach, G., Reppin, C., and Share, G. H.: 1985, *19th Int. Cosmic Ray Conf.* **4**, 126.
Cliver, E. W., Dennis, B. R., Kiplinger, A. L., Kane, S. R., Neidig, D. F., Sheeley, N. R., Jr., and Koomen, M. J.: 1986, *Astrophys. J.* **305**, 920.
Cornwel, T. J. and Evans, K. F.: 1985, *Astron. Astrophys.* **143**, 77.
Debrunner, H., Lackwood, J. A., Ryan, J. M., McConnel, M., Schönfelder, V., Aarts, H., Bennettt, K., and Winkler, C.: 1993, *23th Int. Cosmic Ray Conf.* **3**, 115.
Dulk, G. A. and Marsh, K. A.: 1982, *Astrophys. J.* **259**, 350.
Forrest, G. J. and Chupp, E. L.: 1983, *Nature* **305**, 291.
Forrest, D. J., Vestrand, W. T., Chupp, E. L., Rieger, E., Cooper, J., and Share, G. H.: 1986, *Adv. Space. Res.* **6**, 115.
GLE Data Base for Solar Cycle 22: 1994, Boston College, Institute for Space Research.
Güdel, M., Aschwanden, M. J., and Benz, A. O.: 1991, *Astron. Astrophys.* **251**, 285.
Gueglenko, V. G., Kocharov, G. E., Kovaltsov, G. A., Kocharov, L. G., and Mandzhavidze, N. Z.: 1990, *Solar Phys.* **125**, 91.
Harrison, R. A. and Sime, D. G.: 1989, *J. Geophys. Res.* **94**, 2333.
Harrison, R. A., Wagget, P. W., Bentley, R. D., Phillips, K. J., Bruner, M., Dryer, M., and Simnett, G. M.: 1985, *Solar Phys.* **97**, 387.

Kahler, S. W.: 1984, *Solar Phys.* **90**, 133.
Kahler, S. W.: 1992, *Ann. Rev. Astron. Astrophys.* **30**, 113.
Kai, K., Nakajima, H., Kosugi, T., Stewart, R. T., Nelson, G. J., and Kane, S. R.: 1986, *Solar Phys.* **105**, 383.
Kalmán, B.: 1992, private communication.
Kanbach, G. and 19 co-authors: 1993, *Astron. Astrophys. Suppl. Ser.* **97**, 349.
Karlický, M.: 1992, in Z.Švestka, B. V. Jackson, and M. E. Machado (eds.), *Eruptive Solar Flares, Lecture Notes in Physics* **399**, 171.
Karlický, M. and Zhou Ai-hua: 1993, *Solar Phys.* **146**, 199.
Karlický, M., Aurass, H., and Mann, G.: 1986, *Solar Phys.* **104**, 165.
Kocharov, G. E., Kocharov, L. G., Kovaltsov, G. A., and Mandzhavidze, N. Z.: 1988, Preprint of A.F. Ioffe Physical-Technical Institute, Leningrad, No. 1258.
Kocharov, G. E., Chuikin, E. I., Kocharov, L. G., Kovaltsov, G. A., Melnikov, V. F., Podstrigach, T. S., and Usoskin, I. G.: 1993, *23th Int. Cosmic Ray Conf.* **3**, 123.
Kocharov, L. G., Kovaltsov, G. A., Kocharov, G. E., Chuikin, E. I., Usoskin, I. G., Shea, M. A., Smart, D. F., Melnikov, V. F., Podstrigach, T. S., Armstrong, T. P., and Zirin, H.: 1994, *Solar Phys.* **150**, 267.
Kopp, R. A. and Pneuman, G. W.: 1976, *Solar Phys.* **50**, 85.
Leikov, N. G. and 16 co-authors: 1993, *Astron. Astrophys. Suppl. Ser.* **97**, 345.
Litvinenko, Yu. E. and Somov, B. V.: 1993, *Solar Phys.* **146**, 127.
Litvinenko, Yu. E. and Somov, B. V.: 1995, *Solar Phys.* **158**, 317.
Mandzhavidze, N. Z. and Ramaty, R.: 1992a, *Astrophys. J.* **389**, 739.
Mandzhavidze, N. Z. and Ramaty, R.: 1992b, *Astrophys. J.* **396**, L111.
Mandzhavidze, N., Ramaty, R., Akimov, V. V., and Leikov, N. G.: 1993, *23th Int. Cosmic Ray Conf.* **3**, 119.
Martens, P. C. H.: 1988, *Astrophys. J.* **330**, L131.
NGDC CD, No. 001 A27 005, NOAA, Boulder, 1994.
Ramaty, R., Murphy, R., and Dermer, C. D.: 1987, *Astrophys. J.* **316**, L100.
Ramaty, R. and Mandzhavidze, N.: 1994, in S. Enome and T. Hirayama (eds.), *Proc. Kofu Symposium, NRO Report*, No. 360, 275.
Rompolt, B.: 1984, *Adv. Space Res.* **4**, No. 7, 357.
Rompolt, B.: 1990, *Hvar Obs. Bull.* **14**, 37.
Rompolt, B.: 1992, Proc. XIVth Cons. on Solar Physics, Karpacz, Poland, in press.
Rompolt, B. and Švestka, Z.: 1994, *Adv. Space Res.* **17**, No. 4/5, 115.
Ryan, J. M. and Lee, M. A.: 1991, *Astrophys. J.* **368**, 316.
Ryan, J. and 13 co-authors: 1993, in M. Friedlander, N. Gehrels, and D. J. Macomb (eds.), *AIP Conf. Proc. No. 280, Compton Gamma-Ray Observatory*, AIP, New York, p. 631.
Ryan, J. M. and Vestrand, W. T. (eds.): 1994, *AIP Conf. Proc. No. 294, High Energy Solar Phenomena: A New Era of Spacecraft Measurements*, AIP, New York, p. 246.
Schmieder, B., Hagyard, M. J., Ai Guoxiang, Zhang Hongqi, Kalmán, B., Györi, L., Rompolt, B., Démoulin, P., and Machado, M. E.: 1994, *Solar Phys.* **150**, 199.
Sheeley, N. R., Jr., Howard, R. A., Koomen, M. J., Michels, D. J., Schwenn, R., Mühlhäuser, K. H., and Rosenbauer, H.: 1985, *J. Geophys. Res.* **90**, 163.
Smart, D. F. and Shea, M. A.: 1993, *23th Int. Cosmic Ray Conf.* **3**, 59.
Solar-Geophysical Data: 1991, NOAA, Boulder, Nos. 563, 564, 568.
Somov, B. V.: 1981, *Bull. Acad. Sci. USSR, Phys. Ser.* **45**, 114.
Somov, B. V.: 1992, *Physical Processes in Solar Flares*, Kluwer Academic Publishers, Dordrecht, Holland.
Somov, B. V.: 1994, *Fundamentals of Cosmic Electrodynamics*, Kluwer Academic Publishers, Dordrecht, Holland.
Speiser, T. W.: 1965, *J. Geophys. Res.* **70**, 4219.
Struminsky, A., Matsuoka, M., and Takahashi, K.: 1994, *Astrophys. J.* **429**, 400.
Švestka, Z.: 1989, *Solar Phys.* **121**, 399.
Yun-Tung Lau, Northrop, T. G., and Finn, J. M.: 1993, *Astrophys. J.* **414**, 908.
Zhang, H.-Q. and Chupp, E. L.: 1989, *Astrophys. Space Sci.* **153**, 95.